J. Fluid Mech. (1982), *vol.* 115, *pp.* 165–185
Printed in Great Britain

The instability and breaking of deep-water waves

By W. K. MELVILLE

Institute of Geophysics and Planetary Physics, University of California,
San Diego, La Jolla, and
Massachusetts Institute of Technology, Cambridge

(Received 22 January 1981 and in revised form 11 May 1981)

An experimental study of the evolution to breaking of a nonlinear deep-water wave train is reported. Two distinct regimes are found. For $ak \leqslant 0{\cdot}29$ the evolution is sensibly two-dimensional with the Benjamin–Feir instability leading directly to breaking as found by Longuet-Higgins & Cokelet (1978). The measured side-band frequencies agree very well with those predicted by Longuet-Higgins (1978*b*). It is found that the evolution of the spectrum is not restricted to a few discrete frequencies but also involves a growing continuous spectrum, and the description of the evolution as a recurrence phenomenon is incomplete. It is found that the onset of breaking corresponds to the onset of the asymmetric development of the side bands about the fundamental frequency and its higher harmonics. This asymmetric evolution, which ultimately leads to the shift to lower frequency first reported by Lake *et al.* (1977), is interpreted in terms of Longuet-Higgins' (1978*b*) breaking instability. For $ak \geqslant 0{\cdot}31$ a full three-dimensional instability dominates the Benjamin–Feir instability and leads rapidly to breaking. Preliminary measurements of this instability agree very well with the recent results of McLean *et al.* (1981).

1. Introduction

This paper reports on an experimental study of the evolution to breaking of a uniform deep-water wave train. The processes that may precede and cause deep-water breaking are poorly understood, although significant advances have been made in recent years (see below). The surfaces of natural water bodies are unbroken only in the lightest winds (Melville 1977), with much of the mass, momentum and energy transfer occurring during relative short periods of high winds. It follows that a better understanding of wave breaking is required to understand these processes further. Theoretical difficulties arise through the nonlinearity of the surface boundary condition and the unsteady nature of the flow. Further difficulty arises in so far as breaking may be a transitional phenomenon separating laminar from turbulent flow, the latter introducing its own collection of unsolved problems.

In addition to its role in surface mixing, breaking also serves to limit the amplitude of surface waves and in this context Stokes' (1880) highest wave, incorporating the 120° corner flow, is perhaps the first solution corresponding to a wave at the point of 'incipient breaking'. Stokes' solution was for a *steady* irrotational flow with a free surface. It took almost one hundred years for one of the restrictions of Stokes' solution to be lifted, namely irrotationality. This was done by Banner & Phillips (1974) who proposed that viscous wind-drift layers would exist in the neighbourhood of the

wind-driven surface, leading to an augmentation of the orbital velocity and permitting the fluid velocity to equal the phase velocity at a significantly smaller wave amplitude. The equivalence of fluid and phase velocities, in this steady model, corresponds to the point of incipient breaking. Subsequently Longuet-Higgins & Cokelet (1976) used numerical techniques to follow the evolution of the surface to breaking following an initial pressure perturbation. In addition to demonstrating that pressure perturbations may lead to breaking, Longuet-Higgins & Cokelet's work was noteworthy for introducing a numerical technique to study unsteady surface flows; a serious weakness of Banner & Phillips' (1974) model is the assumption of a steady flow.

Almost a decade earlier Benjamin & Feir (1967) had demonstrated that weakly nonlinear free-surface waves are unstable to side-band instabilities. Their analysis was for a linear perturbation to the weakly nonlinear solutions and predicted exponential growth over a finite band of perturbation frequencies. Employing Whitham's average-Lagrangian method, Lighthill (1967) found that the linear perturbations restabilized for $ak \geqslant 0{\cdot}34$, where a is the wave amplitude and k the wavenumber. At this point ($ak = 0{\cdot}34$) the equations governing the evolution of the wavenumber and amplitude change from elliptic to hyperbolic form. In the hyperbolic regime the group velocity splits into two real characteristics as first noted by Whitham (1965).

Quantitative confirmation of Benjamin & Feir's analysis was claimed by Lake *et al.* (1977) who conducted laboratory experiments on the evolution of nonlinear wave trains. A subsidiary result of their work was the observation that uniform, or nearly uniform, wave trains of large initial steepness may pass through a modulation/demodulation cycle involving wave breaking. While their main concern was not the process of breaking, they had demonstrated that intrinsic hydrodynamic instabilities lead to breaking in the absence of any forcing.

Subsequently Longuet-Higgins (1978*a*, *b*) used a normal-mode analysis to examine the stability of strongly nonlinear waves to small (linear) perturbations. He confirmed the Benjamin–Feir analysis as an asymptotic result, the restabilization first predicted by Lighthill, and also found a new and very strong instability at $ak \simeq 0{\cdot}41$, conjecturing that it corresponded to the initiation of a plunging breaker. The boundary of the unstable region corresponds to the point at which the frequency of the perturbation is zero relative to the unperturbed wave. It is of interest to note that Lighthill's (1967) results show an equivalence of the nonlinear phase velocity and the upper branch of the group velocity at $ak \simeq 0{\cdot}41$ (cf. Lighthill 1978, figures 113, 115). The association of this strong instability with breaking was later confirmed by numerical experiments (Longuet-Higgins & Cokelet 1978) that permitted the assumptions of the linear stability analysis to be relaxed. The numerical solutions were periodic in space with a length of twice the initial wavelength. The numerical results demonstrated that waves having an initial steepness ak as small as 0·25† evolved to breaking with oscillations in both amplitude and wavenumber such that waves finally broke with an individual steepness of about 0·39, somewhat less than the steady limiting steepness of $ak = 0{\cdot}443$.

The experimental and numerical work cited above provides evidence that a uniform train of plane deep-water waves may evolve to breaking through intrinsic

† This was the smallest ak considered in the unstable region.

hydrodynamic instabilities without external forcing. However, the experimental observations by Lake *et al.* (1977) (as they regard breaking) are qualitative and the numerical results of Longuet-Higgins & Cokelet (1978) were constrained by an imposed spatial periodicity of two wavelengths. The experiments reported here were undertaken to provide a more complete description of the processes leading up to breaking, and breaking itself.

It was anticipated initially that the experiment would be two-dimensional; however, it was impossible to generate plane waves for $ak > 0{\cdot}29$. Indeed, a very rapid transition from two- to three-dimensional waves took place. During the course of this work it was found that Su (1980) had observed similar behaviour in a much larger facility and Saffman & Yuen (1980) had interpreted Su's measurements as a bifurcation from the plane-wave solution as found from the Zakharov equation. While the main concern of the experiments reported here was with plane waves, preliminary observations of these three-dimensional effects are given in an appendix.

2. The experiments

The experiments were conducted in the glass channel at Scripps Institution of Oceanography. The channel is 28 m long, 50 cm wide and was filled to a depth, h, of 60 cm. The waves were generated by a hydraulically actuated servo-controlled paddle driven by a sinusoidal signal generator. In all of the experiments reported here the frequency ω_0 was 2 Hz, giving a linear wavenumber $k_0 = 0{\cdot}161$ cm^{-1} and $kh = 9{\cdot}67$, so the waves were deep-water waves ($kh \gg 1$).

A beach of slope 1:20 began at a point 16 m from the paddle and extended for 12 m, the latter half of which was covered with 'horsehair' to provide additional dissipation.

Surface displacements were measured with fine-resistance wave gauges which have been described elsewhere (Flick *et al.* 1979). There appears to be continuing uncertainty regarding the dynamic response of mechanical wave gauges and to our knowledge there is no standard method of calibration. We concluded that the only reliable method was a direct test *in situ*. Preliminary experiments were conducted by generating a strongly modulated wave train having a carrier wave of 2 Hz and measuring the surface displacement in the breaking region with both the wave gauge and high-speed (500 frames/s) cinematography. The height between the crest of the breaking wave and the following trough was measured from the film and compared with the calibrated wave-gauge output. Over a limited series of comparisons (6 breaking waves) the mean error $\bar{\epsilon}$ was 0·5 % with an r.m.s. error of 7 %. The low mean error supports the conclusion that there was virtually no consistent error in the wave-gauge readings, and the larger r.m.s. error was most likely due to the difficulty of reading the (turbulent) crest position from the film. In addition, the wave-gauge records of breaking waves were low-pass filtered in steps of 10 Hz from 10–100 Hz and it was found that the cut-off (whether in the surface displacement or the gauge response) occurred at approximately 50 Hz.

Preliminary experiments showed that the transients following the initiation of paddle motion were long-lived, and influenced by the beach geometry. It was concluded that the initial random perturbations were very small and it required the small multiple reflections from the beach and the paddle to lead to perturbations at the

paddle that were large enough to evolve to breaking in the length of the channel. Measurements were begun approximately 20 min after the paddle was started, by which time the starting transients had disappeared. Data from five wave gauges were sampled continuously for a total of 819·2 s at 100 Hz. The data were recorded on digital tape for subsequent processing. The wave gauges were statically calibrated before and after each series of measurements which lasted from 2 to 4 hours.

In all of these experiments the frequency ω was kept constant and the wave amplitude a was varied. The wave amplitude is defined by

$$a = 0{\cdot}5(\bar{a}_{\max} - \bar{a}_{\min})_{xk_0=41{\cdot}9},$$

where $\bar{a}_{\max}$, $\bar{a}_{\min}$ are averages over approximately 100 waves of the crest and trough elevations respectively. The variable x is the distance downstream from the equilibrium paddle position. The linear wavenumber is denoted by k_0; $xk_0 = 41{\cdot}9$ was the position of the first measuring station. For fixed ω_0, the wavenumber k varies with a and was determined graphically from the tabulated results of Holyer (1979). This contrasts with most theoretical and numerical studies where k is fixed and ω varies with a.

3. Results

3.1. *Preliminary observations*

Ideally, these experiments would be carried out in a much longer channel so that the wave field could dissipate to an evanescent state as $x \uparrow \infty$. However, the wave channel is of finite length and the waves are dissipated by shoaling on a beach as well as by viscosity and breaking in the main body of the channel.† Dissipation at the beach is not complete and some energy, albeit very little, is reflected back towards the wave generator. This reflection is most apparent following the start of wave generation. Groups form first near the head of the wave train and their reflections may be followed back along the channel where they are reflected off the paddle.

For sufficiently large amplitudes the waves underwent a Benjamin–Feir instability leading to breaking, and initially the point at which breaking started moved slowly back along the channel towards the paddle. These starting transients were due to the multiple reflections from the beach slowly increasing at the paddle and providing the initial perturbation for the Benjamin–Feir instability. With some exceptions (see below) a statistically stationary state was achieved after approximately ten round-trips of the channel at the group velocity. Subsequently, the waves evolved to breaking and then went through a region of breaking that ultimately gave way to a region of unbroken waves. The breaking in all cases was 'gentle', with no visible air entrainment except for a very occasional bubble on the surface. The beginning and end of the breaking region could be determined by direct observation to within approximately ± 1 m.

For small-enough initial amplitudes, $ak > 0{\cdot}16$, breaking did not occur in the length of the channel. For slightly larger amplitudes breaking occurred but the process was slowly varying over long time scales such that the point at which breaking began moved slowly in a range of ± 3 m. It is conjectured that this

† Radiation damping by capillary generation may also dissipate the gravity waves.

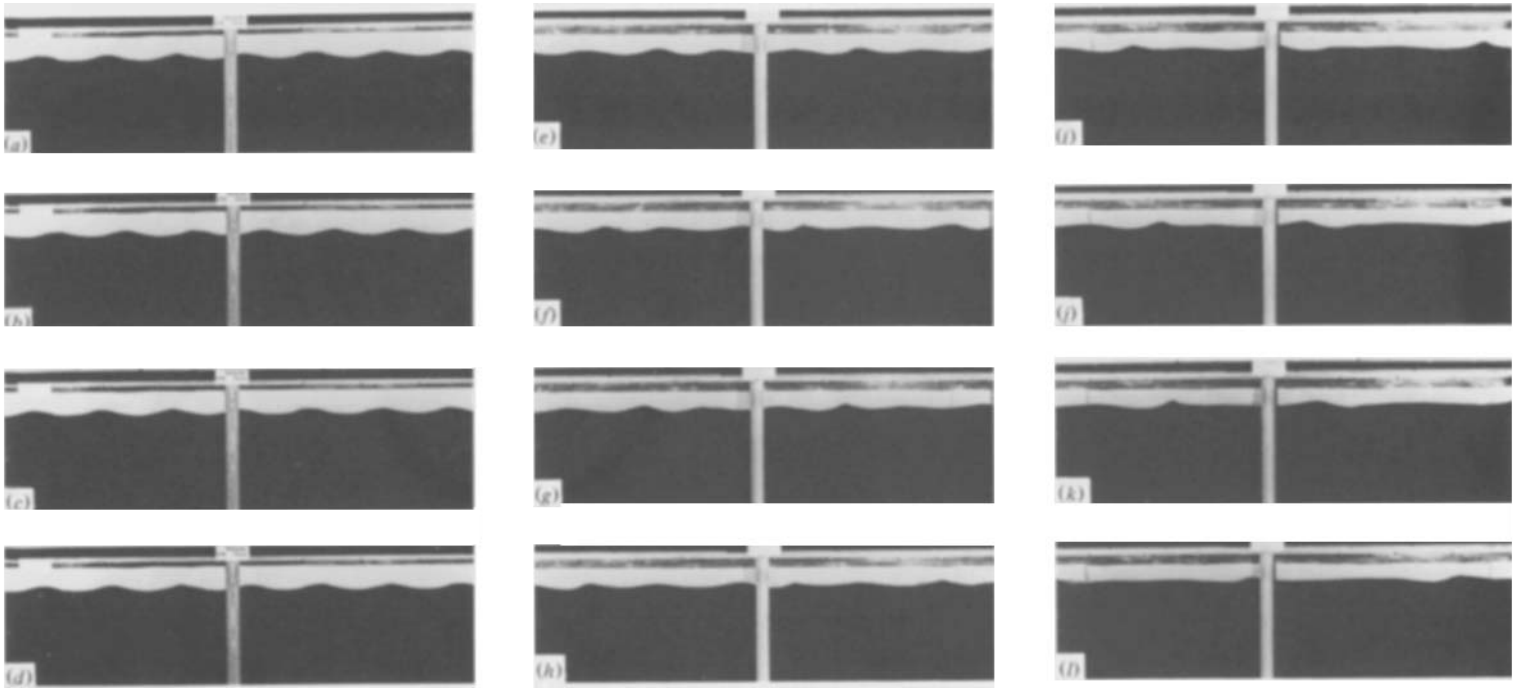

FIGURE 1. Surface profiles for $ak = 0{\cdot}21$. Left-hand column (a–d): $xk_0 = 50$, incident waves. Centre column (e–h): $xk_0 = 195{\cdot}6$, onset of breaking. Right-hand column (i–l): $xk_0 = 256{\cdot}2$, established breaking. Waves propagate from left to right. Tick marks, at extreme top centre, delineate a metre rule for scaling.

behaviour is associated with the weaker attenuation of the beach at smaller wave amplitudes. For a given wave frequency and beach slope the attenuation increases with increasing incident amplitude. For the smaller amplitudes the modulated reflections which propagate with the group velocity may be of sufficient amplitude to produce significant slow modulations of the incident waves.

The incident waves were essentially plane gravity waves, the only obvious perturbation arising from capillary-wave wakes having their origin near the intersection of the gravity-wave crest and the side walls. It was concluded that these result from the disturbance caused by wetting of the side wall near the crest. As a crest passes it wets the side wall, and between crests the surface film drains until the next crest passes by. It appears that the intersection of the draining film and the following wave is the source of the disturbance.

As mentioned above, true three-dimensional effects became evident at sufficiently large amplitudes and these will be discussed in an appendix.

3.2. *Photographic results*

One of the difficulties encountered in comparing theoretical, numerical, and experimental results is the fact that the theoretical studies usually examine the evolution in time of a wave field that is periodic in space, while experiments are most easily conducted for the spatial evolution of a wave field that is periodic in time. The transformation is usually made by using the linear group velocity (see below), but the difficulties associated with the interpretation of the group velocity of nonlinear waves (Peregrine & Thomas 1979) make a direct observation of the spatial evolution of considerable value. To this end we present still photographs of the evolving wave field for $ak = 0{\cdot}21$, $0{\cdot}28$ in figures 1 and 2 respectively. In each case the waves are propagating to the right. The left-hand column shows the incident waves just off the paddle, the centre column shows the region at the onset of breaking, and the right-hand column is in the established-breaking region. Photographs in the same column were taken under exactly the same conditions. For the photographs in the centre and right-hand columns the photographer was asked to shoot to catch breaking events. The relatively short duration of the spilling break makes it a difficult task to catch the waves exactly at breaking in each instance, and the photographs display waves immediately before and after, as well as during, breaking.

Before discussing the photographs in detail a few general observations are in order. The first is the strong temporal periodicity as evidenced by comparison of figures 1 (*j*, *k*) and figures 2 (*g*, *h*). Secondly, the individual breaking waves display a longitudinal asymmetry, with the forward face steeper than the rear, e.g. figure 2 (*h*). Thirdly, there is the very strong modulation in the fully developed breaking region with an almost flat surface between breaking waves, e.g. figures 1 (*l*) and 2 (*l*).

For $ak = 0{\cdot}21$, figure 1, a linear interpolation of Longuet-Higgins' (1980) results for the most unstable mode gives a wavelength of 3·07 times the primary wavelength λ. The non-integral length of the group would preclude simultaneous breaking of waves being observed in the length of channel displayed in the photographs. If, however, the predicted length were a rational number then such behaviour should be evidenced in a sufficiently long channel. Nevertheless, there is some evidence in the photographs (figures 1 (*e*, *g*, *l*)) that the group length is close to 3λ.

For $ak = 0{\cdot}28$, the predicted group length is $2{\cdot}26\lambda$, while the photographic evidence

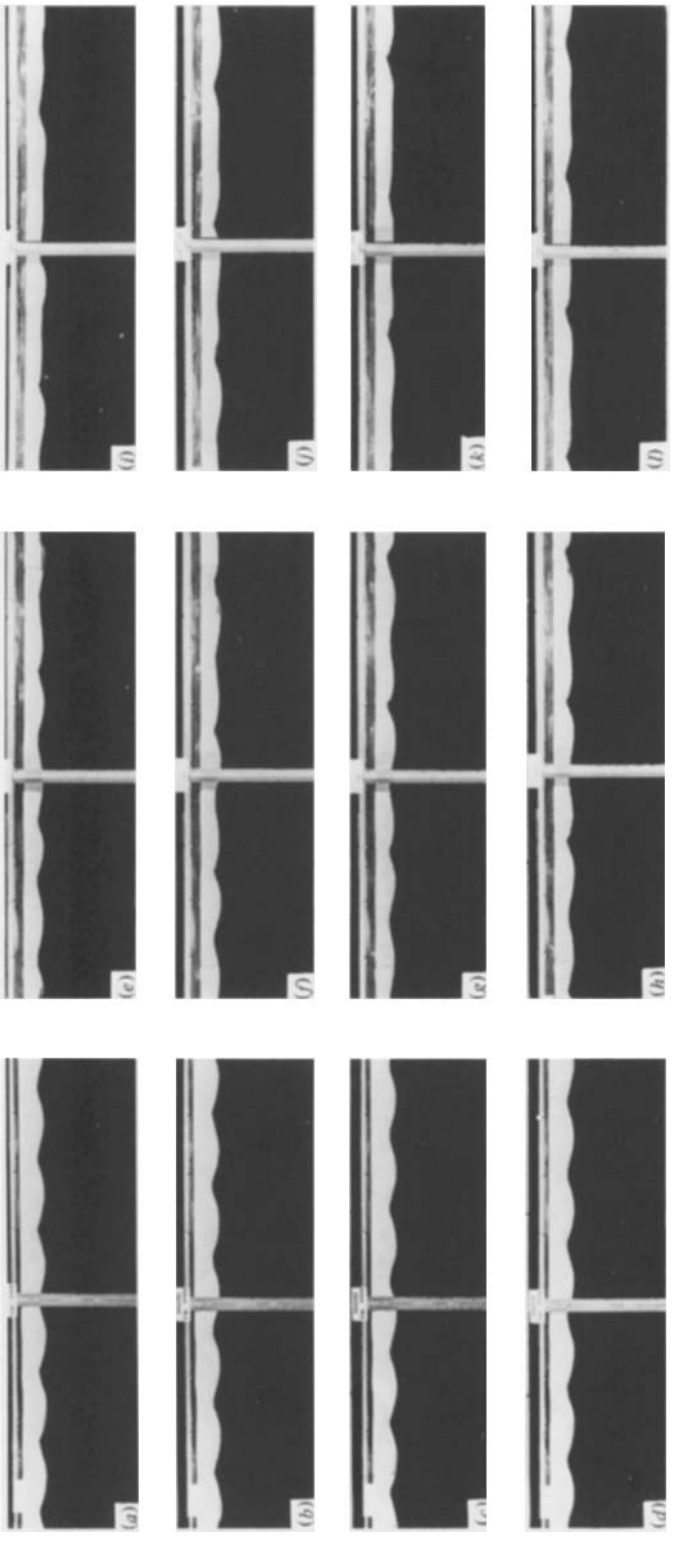

FIGURE 2. Surface profiles for $ak = 0{\cdot}28$. Left-hand column (a–d): $xk_0 = 50$, incident waves. Centre column (e–h): $xk_0 = 167{\cdot}7$, onset of breaking. Right-hand column (i–l): $xk_0 = 226{\cdot}7$, established breaking. Waves propagate from left to right.

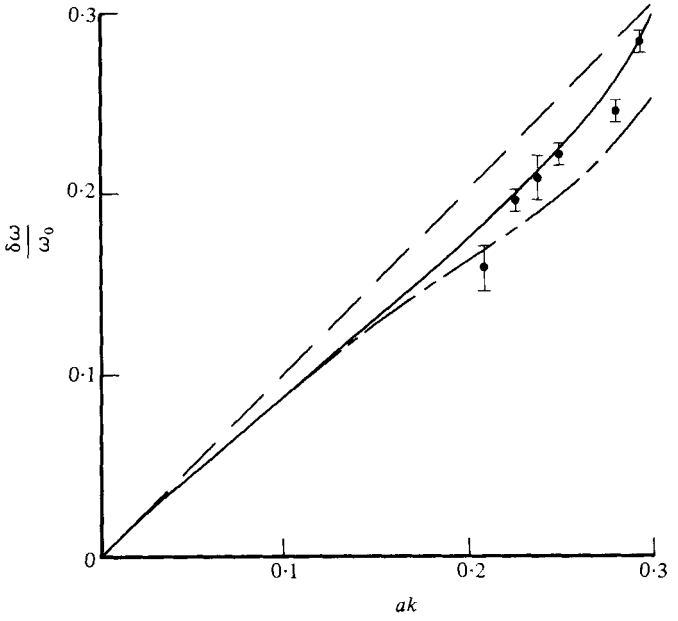

FIGURE 3. Normalized modulation frequency $\delta\omega/\omega_0$ versus ak. ●, measured values with error bars; ———, Benjamin & Feir (1967); ——, Longuet-Higgins (1978*b*, 1980); — — —, Crawford *et al.* (1981). Experiment corresponding to measurement at $ak = 0{\cdot}20$ displayed considerable intermittency.

especially figures 2(*f*, *g*, *l*) shows four groups with every second wave breaking, or near breaking. Given the predicted group lengths, it is not clear why the integral group length should appear so dramatically for $ak = 0{\cdot}28$ and not for $ak = 0{\cdot}21$.

Notwithstanding these differences, these results provide considerable support for the conclusion that the Benjamin–Feir instability is followed by wave breaking in the manner described by Longuet-Higgins & Cokelet (1978). Further, the similarity between the profiles in the fully developed breaking region and at the onset of breaking suggests that the results of numerical models up to the point of breaking may be used to interpret the processes occurring during breaking (see the discussion in §4).

3.3. *Side-band evolution*

The dominant feature of the initial evolution of the wave train is the onset of the Benjamin–Feir instability. Benjamin & Feir's (1967) analysis is asymptotic for $ak \downarrow 0$ and some confusion has arisen from attempts to apply the prediction of the sideband frequency outside its region of validity (Lake *et al.* 1977; Lake & Yuen 1977). Higher-order corrections have been obtained by Dysthe (1979), with a nonlinear Schrödinger equation correct to $O(\epsilon^4)$, and by Crawford *et al.* (1981) with the Zakharov equation; however, predictions of the fastest-growing sideband† by both these methods appear to be quantitatively acceptable only for $ak \lesssim 0{\cdot}15$. As far as we are aware, the only exact predictions up to the limiting wave amplitude are those of Longuet-Higgins (1978*b*). In figure 3 we show the modulation frequency $\delta\omega$ versus ak, along with the predictions of Benjamin & Feir (1967), Crawford *et al.* (1981) and

† Other quantities may be predicted with greater accuracy for larger ak.

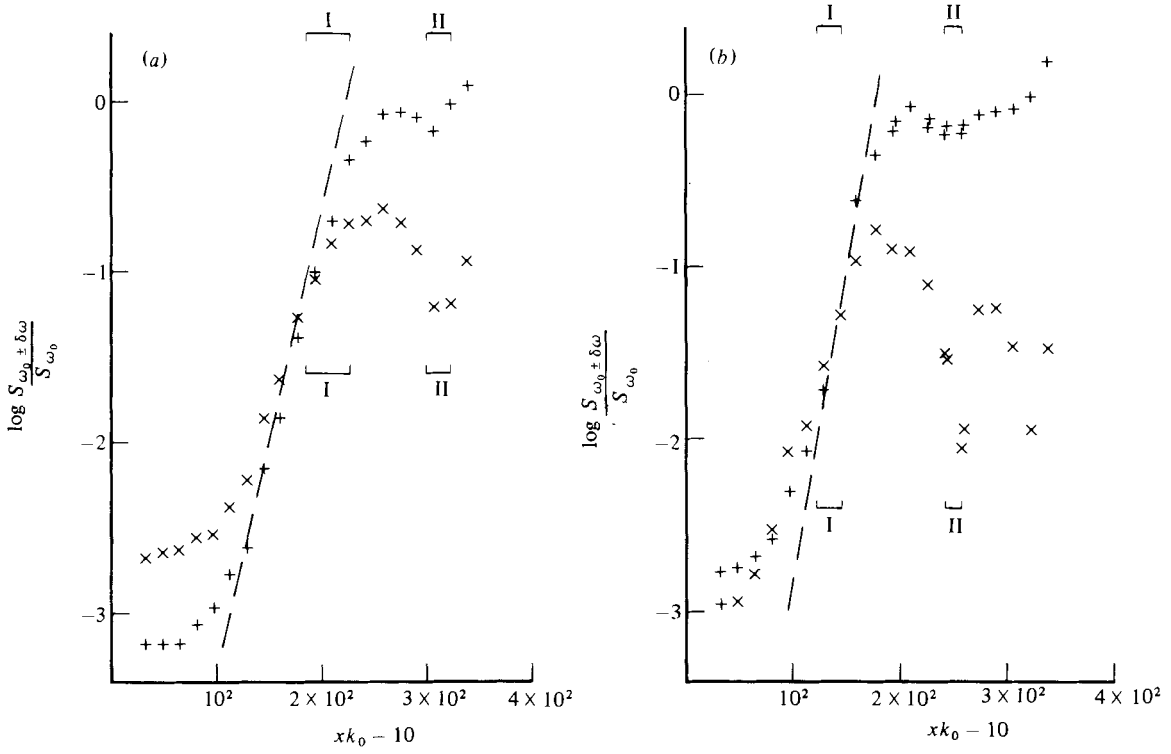

FIGURE 4. Ratio of spectral estimates at side bands $\omega_0 + \delta\omega$ ($\times$) and $\omega_0 - \delta\omega$ ($+$) to that at ω_0, versus xk_0 for: (*a*) $ak = 0{\cdot}233$, (*b*) $ak = 0{\cdot}292$. Regions marked I and II are those in which breaking was observed to begin and end, respectively. The dashed lines are the corresponding side-band growth rates obtained from Longuet-Higgins (1978*b*).

Longuet-Higgins (1978*b*, 1980). Except for the smallest value of ak, the experimental results show very good agreement with the prediction of Longuet-Higgins (1978*b*, 1980), while the asymptotic results, and those based on Zakharov's equation, display comparable errors in the range of the experiments.† The result at $ak = 0{\cdot}20$ corresponds to a set of measurements which displayed considerable intermittent variation in the breaking region, perhaps for the reasons mentioned in §2, and it is only included for completeness.

Constrained by a relatively short wave channel, Lake *et al.* (1977, figure 3) displayed the side-band growth for a series of measurements in which side bands of different amplitudes were forced at the paddle. They then patched the measurements together to obtain the evolution in an effectively longer channel. Given the numerous discrete lines that appear in the spectra we were concerned to confirm that the evolution from essentially random noise was qualitatively similar. Further, we wished to see whether the spectra displayed any gross features corresponding to the onset and cessation of breaking. Following Lake *et al.* (1977) we plot in figure 4 the normalized side-band spectral estimates relative to the estimate at the fundamental frequency versus the distance down the channel, for $ak = 0{\cdot}233$, $0{\cdot}292$. The basic

† Dysthe's (1979) prediction of $\delta\omega$ is worse than that of Crawford *et al.* (1981) and is not shown here.

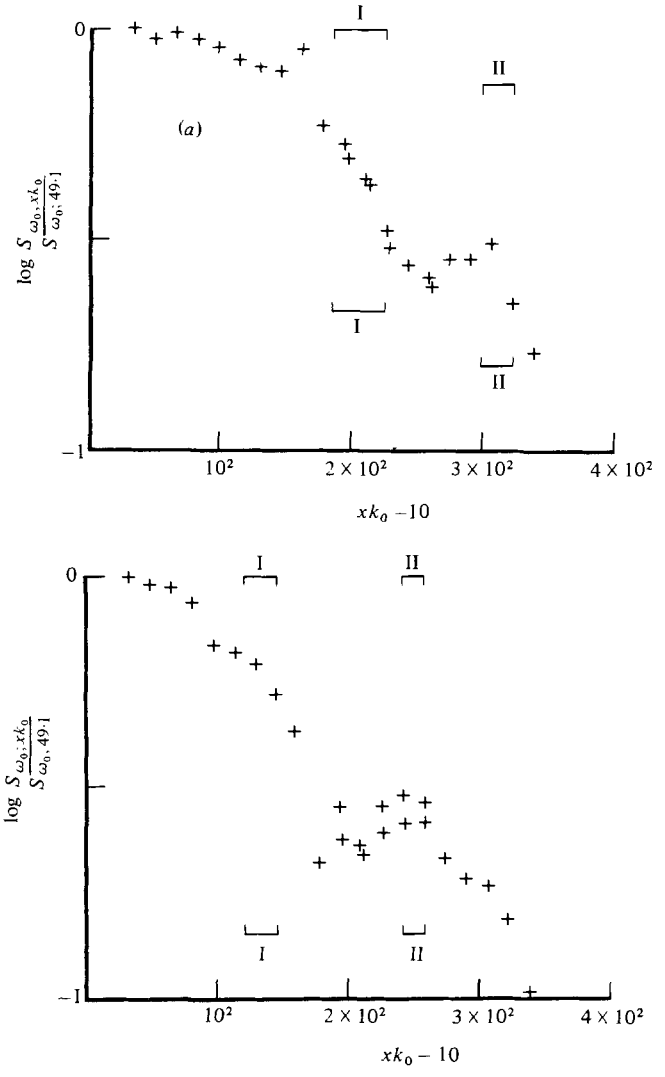

FIGURE 5. Spectral amplitudes at ω_0 normalized to the value at $xk_0 = 41{\cdot}9$ for: (*a*) $ak = 0{\cdot}233$, (*b*) $ak = 0{\cdot}292$. I and II denote the regions in which breaking was observed to begin and end, respectively.

results are strikingly similar to those of Lake *et al.* (1977), but here we have also shown the regions corresponding to the onset and cessation of breaking. In each case (including results not shown here) the side bands are initially of unequal amplitude but equilibrate on moving down the channel. Subsequently, the amplitudes diverge and in each case the divergence occurs in the neighbourhood of the onset of wave breaking, with the lower side band $\omega_0 - \delta\omega$ reaching the larger amplitude a little after the upper side band $\omega_0 + \delta\omega$ reaches its smaller local maximum. Subsequently, both fall to local minima before growing again. (For $ak = 0{\cdot}292$ there is some evidence of a second local minimum of the upper sideband.) In each case studied this local minimum corresponds to the cessation of breaking. In each case breaking has been accompanied by a reduction in the amplitude of the upper side band relative to the

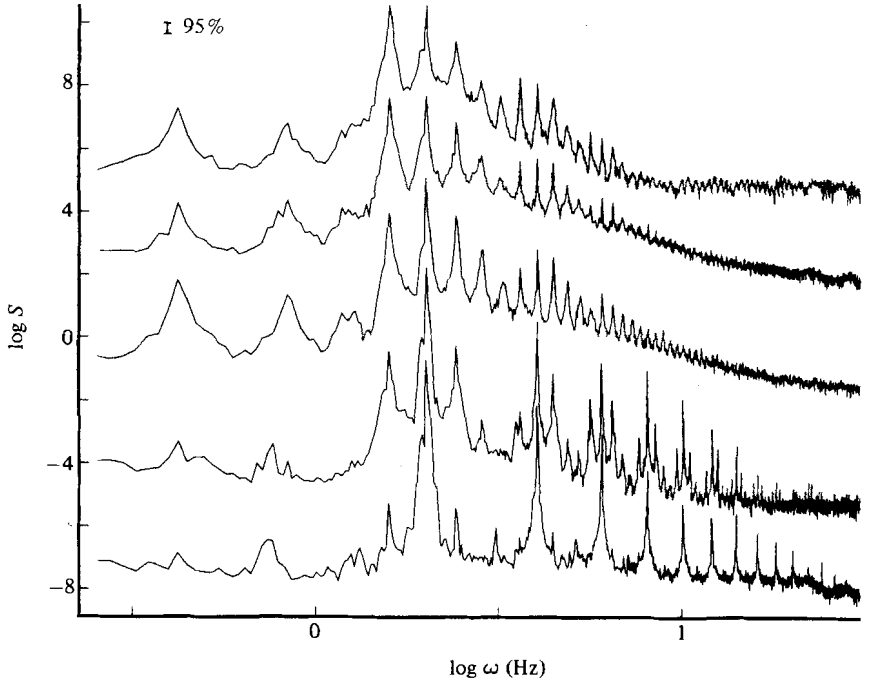

FIGURE 6. Surface-displacement spectra at xk_0 = 41·9, 138·6, 203·0, 282·6, 348·1, for ak = 0·233. Spectra are sequentially offset by $3n$, $n = 0, 1, \ldots, 4$. Resolution bandwidth = 0·0244 Hz; Nyquist frequency = 50 Hz; 40 degrees of freedom. I 95 % confidence interval.

lower side band. In addition, after breaking, the lower side band has grown to an amplitude greater than that of the fundamental frequency ω_0. This is the shift to lower frequency first discovered by Lake *et al.* (1977).

Also shown in figure 4 are the growth rates predicted by Longuet-Higgins (1978*b*) based on the wave amplitude at xk_0 = 41·9. The agreement appears to be good; however, it is not clear that such comparisons are terribly meaningful when the amplitude of the fundamental frequency varies as shown in figure 5. Here we have plotted the normalized spectral estimate of the fundamental frequency, relative to that at xk_0 = 41·9, versus xk_0. Also shown are the regions corresponding to the onset and cessation of breaking. The initial decrease results from dissipation as well as transfer of energy to the side bands. Unfortunately it is not possible to make an accurate determination of the dissipation from causes other than breaking (see Miles 1967). These include viscous dissipation at the boundaries, surface contamination, capillary-wave generation and capillary hysteresis, all of which would lead to a monotonic decrease in the curves. Each curve displays an initial decrease to a local minimum, which corresponds approximately to the position of the local maxima in the side bands (cf. figure 4), before increasing to a local maximum, which corresponds to the local minima in the sidebands. Finally, a region of decreasing amplitude is measured. In contrast to the side-band amplitudes it is only the cessation of breaking that is coincident with a major feature of these curves: the local maxima.

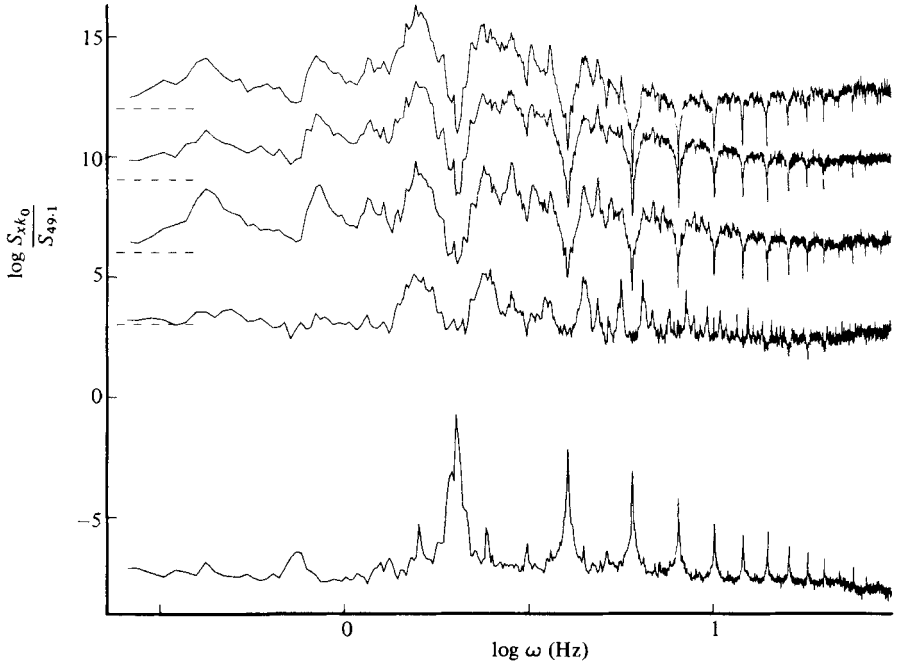

FIGURE 7. Surface-displacement spectrum for $ak = 0{\cdot}233$, $xk_0 = 41{\cdot}9$ and ratios of spectra at $xk_0 = 138{\cdot}6, 203{\cdot}0, 282{\cdot}6, 348{\cdot}1$ to that at $xk_0 = 41{\cdot}9$ (*cf.* figure 6). Curves sequentially offset by $3n$, $n = 0, 1, \ldots, 4$. All technical data as in figure 6. Note the growth of the continuous spectrum about ω.

3.4. *Spectral evolution*

The evolution of the side bands described in §3.3 is important, but the full spectra offer a much more complicated picture of the evolution of the wave train. We consider in some detail the spectra for $ak = 0{\cdot}233, 0{\cdot}292$.

Figure 6 shows the spectra at $xk_0 = 41{\cdot}9, 138{\cdot}6, 203{\cdot}0, 282{\cdot}6, 348{\cdot}1$, for $ak = 0{\cdot}233$. The first two spectra are in the region before breaking, the third and fourth are in the breaking region, and the fifth is just downstream of the breaking region. The first spectrum, at $xk_0 = 41{\cdot}9$, displays significant peaks at $\delta\omega$, ω_0, $\omega_0 \pm \delta\omega$, $2\omega_0$, $3\omega_0$, ..., $n\omega_0$; with n an integer. There is also a peak near $2\delta\omega$. In the second spectrum additional significant peaks are evident at $n\omega_0 \pm \delta\omega$; evidence of the modulation of the higher harmonics at the frequency $\delta\omega$. The next spectrum is at the beginning of the breaking region, where a number of changes are apparent. The peak at $\delta\omega$ has become more pronounced and that *near* $2\delta\omega$ has shifted *to* $2\delta\omega$. Both of these features reflect the increased modulation of the wave train (see figure 1). There has been a relatively broad-band increase in the continuous spectrum. Numerous lines in the discrete spectrum have become more significant; for example, the peaks at $\omega_0 + 2\delta\omega$, $n(\omega_0 \pm \delta\omega)$. Further, the lines evident earlier at the higher frequencies (> 10 Hz, say) have disappeared in the continuous spectrum. The next spectrum shows the growth of the lower sideband relative to the upper sideband (cf. figure 4) and a further destruction of the discrete lines at higher frequencies. The last spectrum shows a return of some of the lines that decreased in the breaking region. These relative changes are shown more clearly in figure 7, where the spectrum at $xk_0 = 41{\cdot}9$, and the ratios between

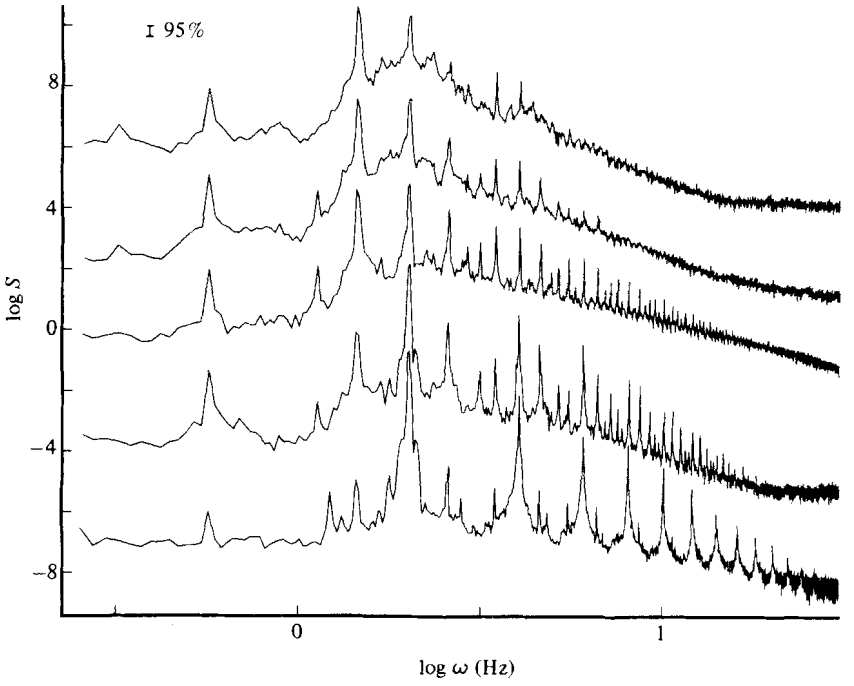

FIGURE 8. Surface-displacement spectra at xk_0 = 41·9, 122·5, 203·0, 283·6, 348·1, for ak = 0·292. See caption of figure 6 for details. Note the loss of the higher-frequency lines and the growth of the continuous spectrum as xk increases. The first and second curves are ahead of the breaking region, and the fourth and fifth are beyond the breaking region.

the spectra at xk_0 = 138·6, 203·0, 283·6, 348·1 and the spectrum at xk_0 = 41·9 are displayed. This figure shows the features described above, most notably the broad-band increase in spectral density and the decrease in the primary wave and its higher harmonics.

Corresponding results for ak = 0·292 are shown in figure 8 for xk_0 = 41·9, 122·5, 203·0, 283·6, 348·1, and the same qualitative description applies.

It is instructive to examine the breaking region in more detail as shown for ak = 0·292 in figure 9(*a*, *b*). Figure 9(*a*) shows the spectrum at xk_0 = 122·5 (just before breaking), 154·7, 186·9, 219·1, and 251·4 (at the end of breaking) and figure 9(*b*) shows the spectrum at xk_0 = 122·5 and the corresponding ratios at xk_0 = 154·7, 186·9, 219·1, 251·4. Reference to figure 4, and the large gradients shown there near the onset and end of breaking, and the imprecision in defining the onset and end of breaking, all militate against a good quantitative estimate of the net effect of breaking on the spectral evolution. Nevertheless, figure 9 displays some strong qualitative features. In particular, there is a marked asymmetry between the upper and lower side bands of not only the fundamental frequency ω_0 but also its higher harmonics $n\omega_0$ showing a decrease of the upper side bands relative to the lower side bands. This is shown most clearly for xk_0 = 219·1, 251·4. It should be noted that some of this asymmetry is evident in the initial spectrum at xk_0 = 122·5. These results show that the harmonics $n\omega_0$ and their upper side bands are most affected in the breaking region.

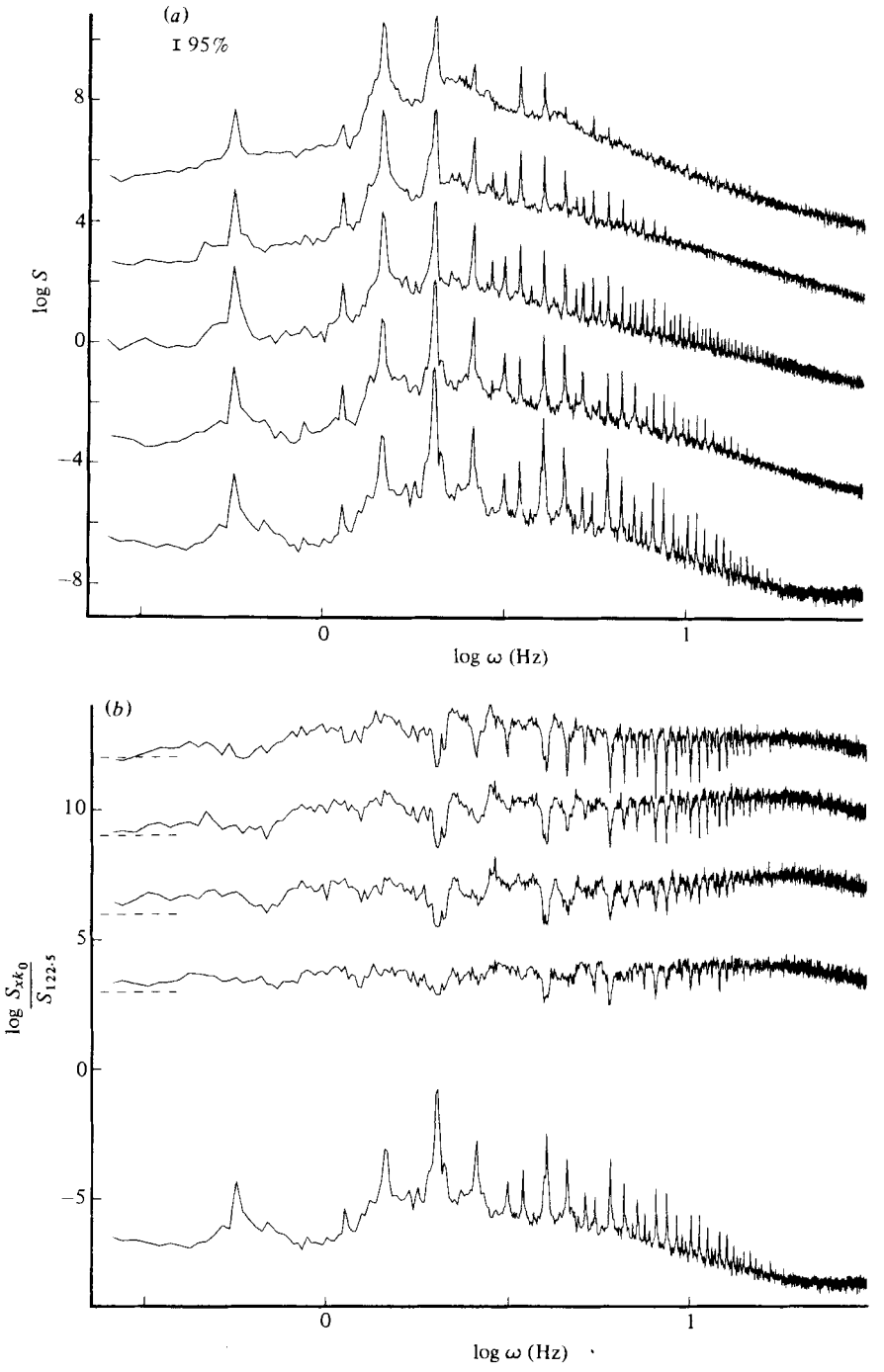

FIGURE 9. (*a*) Surface-displacement spectra for $ak = 0{\cdot}292$ at $xk_0 = 122{\cdot}5$ (just before breaking region), 154·7, 186·9, 219·1 (in the breaking region), and 251·4 (at the end of the breaking region). Curves are offset by $3n$, $n = 0, 1, \ldots, 4$. All technical data as in figure 6. Note the growth and destruction of the dense, discrete, higher-frequency lines. (*b*) Spectrum at $xk_0 = 122{\cdot}5$ and normalized ratios at $xk_0 = 154{\cdot}7$, 186·9, 219·1, 251·4. Note the asymmetry about $n\omega_0$ (n integer).

4. Discussion

Our measurements show that for ak in the range 0·16–0·29 a uniform deep-water wave train undergoes a Benjamin–Feir instability which ultimately leads to breaking. Our measurements agree very well with the modulation frequency predicted by Longuet-Higgins (1978*b*) and show that the asymptotic results of Benjamin & Feir, and results based on the Zakharov equation, display comparable errors over a significant range of wave amplitudes.

Our measurements of the side-band evolution agree qualitatively with those of Lake *et al.* (1977) and show a marked asymmetry between the upper and lower side bands which leads to the lower side band increasing to an amplitude greater than that of the primary wave. However, our observations also show that the onset of the asymmetry corresponds to the onset of wave breaking. A detailed examination of the spectra shows that this asymmetry extends to the higher harmonics of the primary wave and that there is a marked reduction of the energy in these upper side bands in the breaking region. The spectra also show that a continuous spectrum evolves and that a description in terms of a discrete spectrum only is at best an approximation. It should be remembered that the wave train is unstable to a band of frequencies rather than a few discrete lines.

The photographic evidence, especially for $ak = 0{\cdot}292$, shows a remarkable qualitative agreement with the numerical solution of Longuet-Higgins & Cokelet (1978). The photographs also show that the profiles well inside the breaking region are comparable with the computed profiles. This suggests that the numerical results may be used to interpret not only the processes before breaking but also those in the breaking region.

With this assumption we believe that the asymmetric development in the breaking region and the shift to lower frequency may be interpreted in terms of Longuet-Higgins' (1978*b*) and Longuet-Higgins & Cokelet's (1978) findings.

It is noteworthy that the Longuet-Higgins instability, unlike the Benjamin–Feir instability, is *not* symmetric in the side bands, but arises at the junction of the upper side band and the primary wave. In addition, near breaking, the instability is strongly localized and thus would require the generation of numerous Fourier components at $n\delta\omega$, with n an integer. Such components may result from interaction between the higher harmonics of ω_0, $(\omega_0 \pm \delta\omega)$; i.e. $n\omega_0$ and $n(\omega_0 + \delta\omega)$. In the breaking region the energy contained in the higher frequencies $n\delta\omega$ will either be dissipated or scattered into the continuous spectrum. This energy may be replenished by transfer from $n\omega_0$ and $n(\omega_0 + \delta\omega)$, which in turn comes ultimately from the components ω_0 and $\omega_0 + \delta\omega$. This description is consistent with the measured spectra and can explain the shift to lower frequency as the waves pass through the breaking region. The lower side band is not directly involved in the breaking instability and the lower side band $\omega_0 - \delta\omega$ of the fundamental frequency ω_0 will continue to grow as shown by the numerical results of Lake *et al.* (1977).

It should be noted that while Lake *et al.* (1977) were unable to provide a satisfactory explanation of the shift to lower frequency they did conclude that capillary generation or breaking was observed in every case where a shift was measured. They suggested that the shift may be associated with dissipation, but considered it unlikely that dissipative effects could be so selective over the relatively small frequency

difference between ω_0 and $\omega_0 \pm \delta\omega$. However, the breaking instability is evidently very selective, and if it is this perturbation which causes breaking then it is almost certain that it is this perturbation that is most effectively destroyed (dissipated).

A partial recurrence occurs with both upper and lower side bands decreasing to local minima, that correspond to the end of breaking, before they begin to increase again. In the absence of breaking we would expect recurrence to occur at approximately twice the distance required for the sidebands to reach their maxima (see Lake *et al.* 1977, figure 9). However, growth of the continuous spectrum casts considerable doubt on the relevance of models which seek to describe the end state of the evolution as a series of Fermi–Pasta–Ulam recurrences. If the nonlinearity ultimately leads to breaking, as it does here, then consideration of the long-time evolution in the absence of breaking is an unrealizable idealization which will lead to a qualitatively different end state. The present results suggest that the wave train may pass through a series of partial recurrences tending to lower frequency while the continuous spectrum continues to grow. It is then likely that the discrete spectrum ultimately disappears into the continuous spectrum.

The above discussion applies to $ak \leqslant 0{\cdot}29$. For larger amplitudes the experiments display the onset of a strong three-dimensional instability. The limited measurements reported in the appendix show good agreement with the predictions by McLean *et al.* (1981) for the transition from two- to three-dimensional instability, and of the transverse wavenumber. Results based on the Zakharov equation appear to be only qualitatively correct in both cases.

Finally, it should be stressed that, while the results here have been compared with the predictions for deep-water waves, the forced waves in these experiments (those generated by the modulation of the primary wave train) are only marginally so, having δkh in the range 3–5. This does not appear to have led to any significant qualitative differences from the true deep-water case; however, for fixed h, $\delta kh \downarrow 0$ as $ak \downarrow 0$ and so care should be exercised in studies of weakly nonlinear waves, especially in the laboratory.

John Miles' initial encouragement and support made this work possible. My colleagues at the Hydraulics Laboratory of the Scripps Institution of Oceanography, Mike Butler, Charley Coughran and John Powell, all contributed to the experiments. I am indebted to Larry Ford and his colleagues for their skill and patience in producing the photographic work shown here. Dr Henry Yuen kindly made available preprints of recent work from the TRW group. This work was supported by National Science Foundation Grants OCE 77-24005 and OCE 80-09461.

Appendix

For $ak \leqslant 0{\cdot}29$ the approach to breaking was essentially two-dimensional. However, in the breaking region, there was some evidence of three-dimensional effects. Moving with a wave group, the first breaking region was sensibly uniform across the channel but, as the group passed through the breaking region, a weak three-dimensionality developed, with the break occurring alternately in the centre and at the sides of the channel. This pattern is evidenced in figures 10 and 11. These photo-

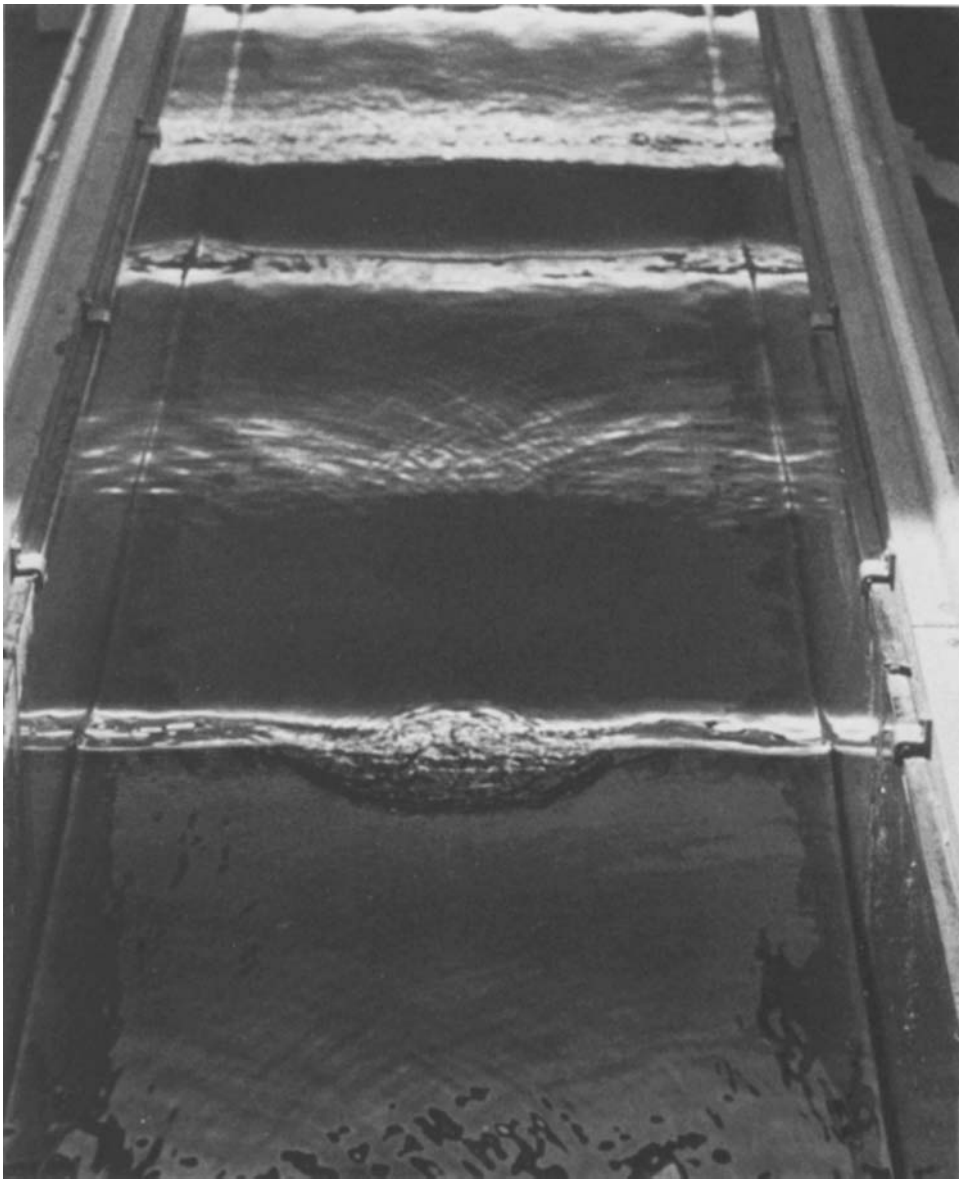

FIGURE 10. View of a breaking wave looking back towards the wave generator; $ak = 0{\cdot}21$. Note that the wave is only breaking in the centre of the channel.

graphs were taken looking back up the channel towards the wave generator. Figure 10 shows the spilling region in the centre of the channel while figure 11 shows the spilling region at the sides of the channel. Low-pass filtering of surface displacement records showed that the spilling region becomes discernible at frequencies greater than 10–20 Hz. This is much larger than the fundamental frequency of 2 Hz and thus this particular three-dimensionality may be regarded as weak.

These weak three-dimensional effects were confined to amplitudes $ak \leqslant 0{\cdot}29$. For slightly larger amplitudes, strong three-dimensional effects arose intermittently

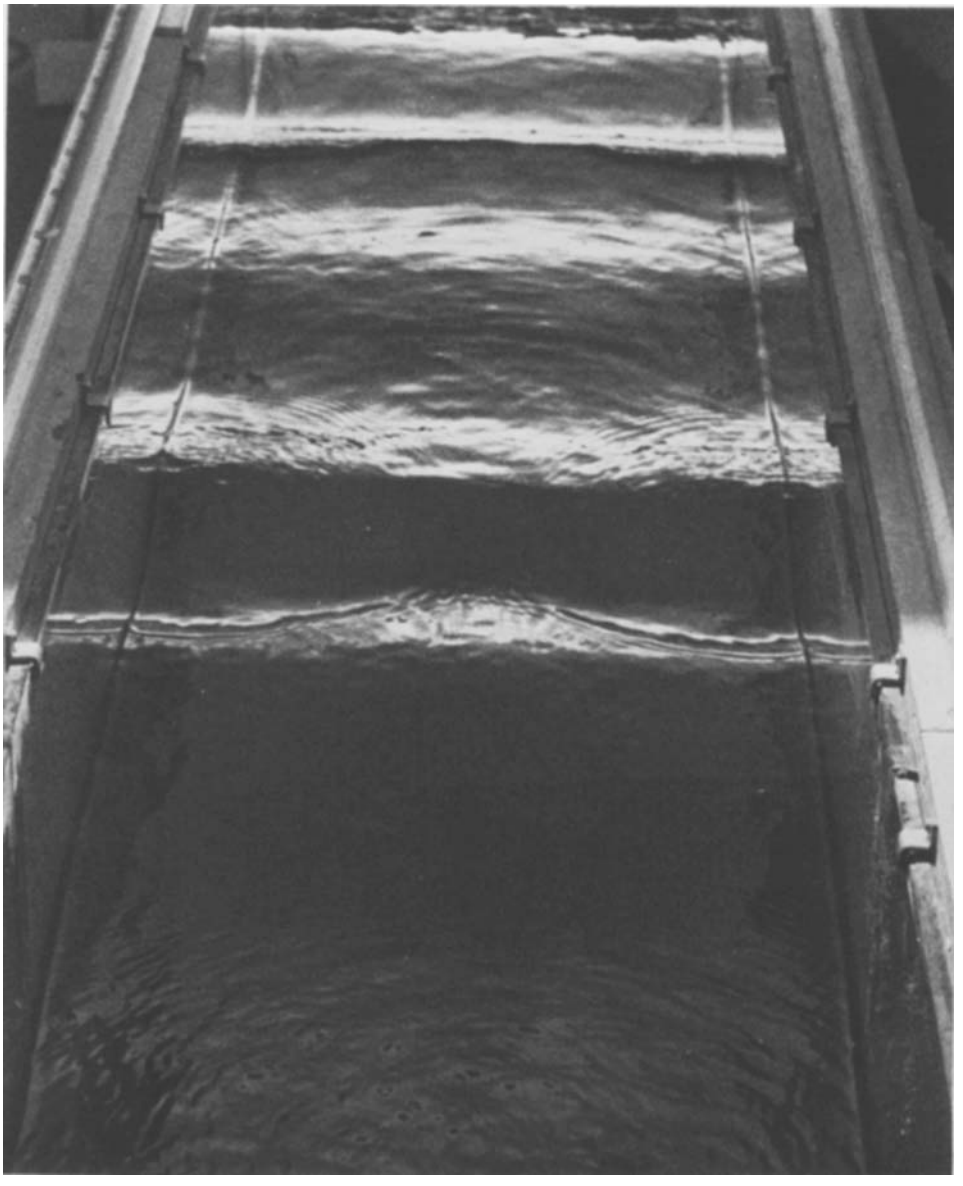

FIGURE 11. Same conditions as figure 10. Note the wave breaking at the sides of the channel in the upper part of the photograph and the capillary waves generated by breaking in the foreground.

within 10 wavelengths of the wave generator; the intermittency undoubtedly being due to very-low-frequency oscillations in the tank. For $ak \geqslant 0{\cdot}31$ the three-dimensional effects appeared to dominate the Benjamin–Feir instability. The three-dimensional pattern took the form of crescent-shaped perturbations riding on the basic waves. These are clearly shown in figure 12. The predominant wavelength of the perturbation was two primary wavelengths (e.g. figures 12*a*, *c*); however, counter examples are evident (figures 12*b*, *d*). In addition, the velocity of the perturbation appeared to be very close to the phase speed of the primary wave; observations

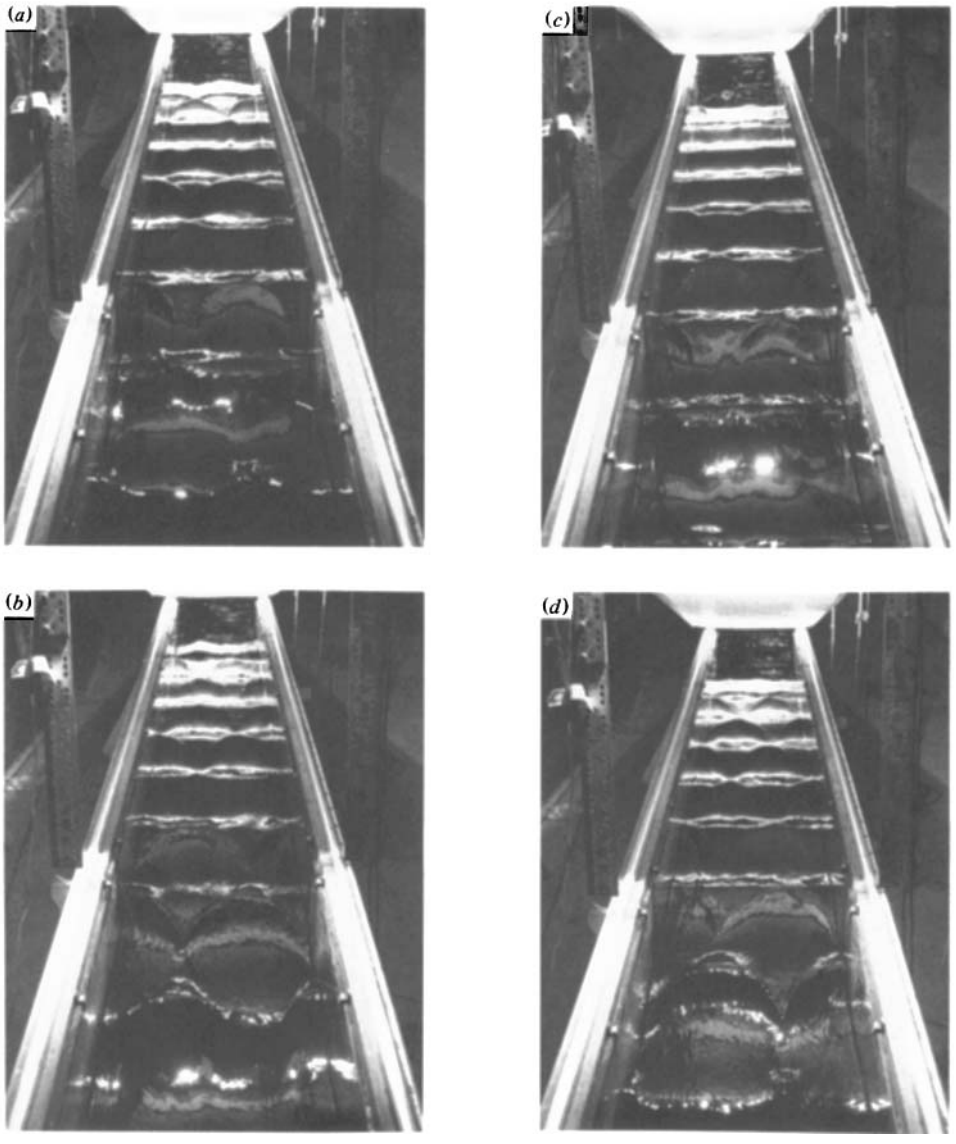

FIGURE 12. Three-dimensional instability of deep-water waves looking downstream. Left-hand column (a, b): $ak = 0{\cdot}315$. Right-hand column (c, d): $ak = 0{\cdot}321$.

showed such phase-locking for distances of approximately 10 primary wavelengths down the channel.

At the head of the crescent, wave breaking and capillary-wave generation were evident for 20–30 primary wavelengths down the channel from the wave generator.

During the course of this work it was learned that Su (1980) had also observed these crescent-shaped perturbations and Saffman & Yuen (1980) had interpreted them as evidence of a bifurcation from the uniform two-dimensional wave train.

Subsequently, McLean *et al.* (1981) undertook a numerical study of the stability of the full water-wave equations to linear three-dimensional disturbances. They found two classes of instability. Class I corresponds to Phillips (1977) 'figure 8'

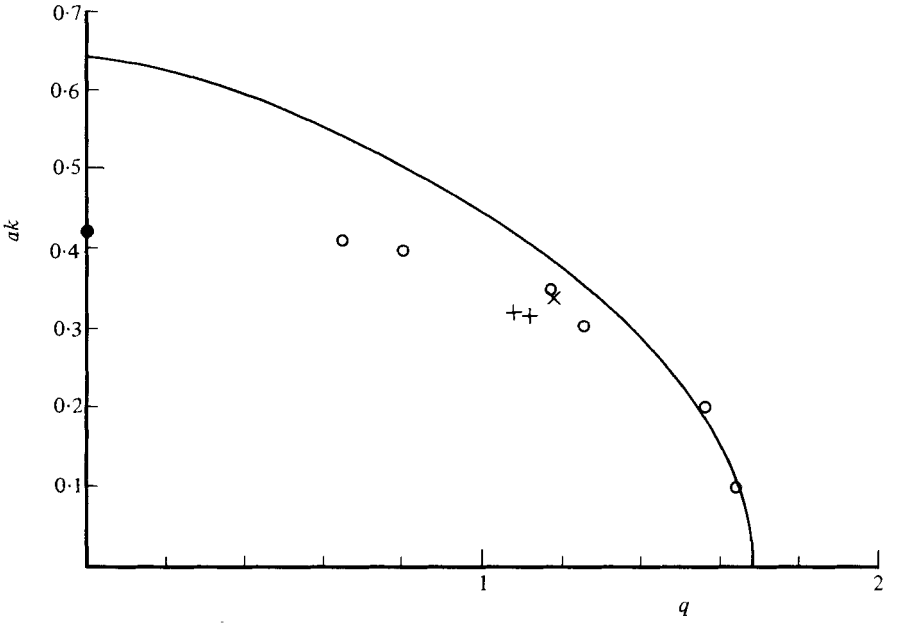

FIGURE 13. Normalized transverse wavenumber q of most unstable subharmonic perturbation for normalized longitudinal wavenumber $p = 0{\cdot}5$. ——, Saffman & Yuen (1981); ○, McLean *et al.* (1981); ×, Su (1981); +, measurements taken from figure 12; ●, Longuet-Higgins (1978*b*).

resonant diagram and the maximum growth rate is always associated with two-dimensional disturbances. Class II is fully three-dimensional; the maximum instability always occurs for $p = 0{\cdot}5$ and $q \neq 0$ for all but the largest ak, where p and q are the ratios of the longitudinal and transverse perturbation wavenumbers, respectively, to the primary wavenumber.† For $p = 0{\cdot}5$ the instability is co-propagating (i.e. the velocity of the perturbation is equal to the phase velocity of the primary wave) in agreement with our observations. Class II includes Longuet-Higgins' (1978*b*) breaking instability as a special case. McLean *et al.* (1981) found that class I had the larger maximum growth rates for $ak \leqslant 0{\cdot}28$, and class II dominated for larger ak. This is in good agreement with our observation that the evolution of the wave train was essentially two-dimensional for $ak \leqslant 0{\cdot}29$. Finally, in figure 13 we have plotted measurements taken from figure 12 along with the points of maximum growth rate of class II instability predicted by McLean *et al.* (1981). In addition we have plotted the corresponding curve predicted by the approximate analysis of Saffman & Yuen (1981), and an experimental point attributed by them to Su (1981).‡

† McLean *et al.* (1981) claimed that the maximum instability always occurs for $q \neq 0$; however, a referee pointed out that Longuet-Higgins' (1978*b*, figure 2) result at $ak = 0{\cdot}421$ ($q = 0$) (beyond their range of calculation) displays a growth rate greater than the largest growth rate presented by McLean *et al.* (1981).

‡ I have not viewed Su's (1981) paper.

REFERENCES

BANNER, M. L. & PHILLIPS, O. M. 1974 On small-scale breaking waves. *J. Fluid Mech.* **65**, 647–657.

BENJAMIN, T. B. & FEIR, J. E. 1967 The disintegration of wave trains in deep water. Part 1. Theory. *J. Fluid Mech.* **27**, 417–430.

CRAWFORD, D. R., LAKE, B. M., SAFFMAN, P. G. & YUEN, H. C. 1981 Stability of weakly nonlinear deep-water waves in two and three dimensions. *J. Fluid Mech.* **105**, 177–191.

FLICK, R. E., LOWE, R. L., FREILICH, M. H. & BOYLLS, J. C. 1979 Coastal and laboratory wave-staff system. In *Proc. Oceans* 79, *I.E.E.E. and Mar. Tech. Soc.*, pp. 623–625.

HOLYER, J. 1979 Large-amplitude progressive interfacial waves. *J. Fluid Mech.* **93**, 433–448.

LAKE, B. M. & YUEN, H. C. 1977 A note on some nonlinear water-wave experiments and the comparison of data with theory. *J. Fluid Mech.* **83**, 75–81.

LAKE, B. M., YUEN, H. C., RUNGALDIER, H. & FERGUSON, W. E. 1977 Nonlinear deep-water waves: theory and experiment. Part 2: Evolution of a continuous wave train. *J. Fluid Mech.* **83**, 49–74.

LIGHTHILL, M. J. 1967 Some special cases treated by the Whitham theory. *Proc. R. Soc. Lond.* A **299**, 28–53.

LIGHTHILL, M. J. 1978 *Waves in Fluids.* Cambridge University Press.

LONGUET-HIGGINS, M. S. 1978*a* The instabilities of gravity waves of finite amplitude in deep water. I. Superharmonics. *Proc. R. Soc. Lond.* A **360**, 471–488.

LONGUET-HIGGINS, M. S. 1978*b* The instabilities of gravity waves of finite amplitude in deep water. II. Subharmonics. *Proc. R. Soc. Lond.* A **360**, 489–505.

LONGUET-HIGGINS, M. S. 1980 Modulation of the amplitude of steep wind waves. *J. Fluid Mech.* **99**, 705–713.

LONGUET-HIGGINS, M. S. & COKELET, E. D. 1976 The deformation of steep surface waves on water. I. A numerical method of computation. *Proc. R. Soc. Lond.* A **350**, 1–26.

LONGUET-HIGGINS, M. S. & COKELET, E. D. 1978 The deformation of steep surface waves on water. II. Growth of normal-mode instabilities. *Proc. R. Soc. Lond.* A **364**, 1–28.

MCLEAN, J. W., MA, Y. C., MARTIN, D. U., SAFFMAN, P. G. & YUEN, H. C. 1981 Three-dimensional instability of finite-amplitude water waves. *Phys. Rev. Lett.* **46**, 817–820.

MELVILLE, W. K. 1977 Wind stress and roughness length over breaking waves. *J. Phys. Ocean* **7**, 702–710.

MILES, J. W. 1967 Surface-wave damping in closed basins. *Proc. R. Soc. Lond.* A **297**, 459–475.

PEREGRINE, D. H. & THOMAS, A. P. 1979 Finite-amplitude deep-water waves on currents. *Phil. Trans. R. Soc. Lond.* A **292**, 371–390.

PHILLIPS, O. M. 1977 *The Dynamics of the Upper Ocean.* Cambridge University Press.

SAFFMAN, P. G. & YUEN, H. C. 1980 Bifurcation and symmetry breaking in nonlinear dispersive waves. *Phys. Rev. Lett.* **44**, 1097–1100.

SAFFMAN, P. G. & YUEN, H. C. 1981 Three-dimensional deep-water waves: calculation of steady symmetric wave pattern. Submitted to *J. Fluid Mech.*

STOKES, G. G. 1880 Supplement to a paper on the theory of oscillatory waves. *Mathematical and Physical Papers*, vol. 1, pp. 314–326. Cambridge University Press.

SU, M. Y. 1980 Experiments on water-wave breaking on deep water. Part I: Three-dimensional subharmonic instability (unpublished manuscript).

SU, M. Y. 1981 Three-dimensional deep-water waves. Laboratory experiments on spilling breakers. Submitted to *J. Fluid Mech.*

WHITHAM, G. B. 1965 A general approach to linear and nonlinear dispersive waves using a Lagrangian. *J. Fluid Mech.* **22**, 273–283.